DIFFRACTION OF THERMAL WAVES IN LIQUID HELIUM II

Thesis by

James E. Mercereau

In Partial Fulfillment of the Requirements

For the Degree of

Doctor of Philosophy

California Institute of Technology

Pasadena, California

1959

ACKNOWLEDGEMENTS

The concept of a thermal grating is due entirely to Professor John R. Pellam to whom I am indebted for encouragement and guidance throughout this investigation.

I wish to express gratitude to the Howard Hughes Research Laboratories for a fellowship 1954-1956, 1958-1959 and to the Bell Telephone Laboratories for a fellowship 1956-1958.

ABSTRACT

Diffraction effects in thermal radiation have been produced in liquid helium II by means of a thermal grating radiating a primary (zero-order) beam accompanied by higher order beams at appropriate "Bragg" angles. These results at once demonstrate unambiguously the true wave nature of this thermal wave propagation and its conformity to Huygens' principle in the most demanding test to which second sound has been subjected. The general nature of the angular pattern, including the fine structure, conforms to the requirements of diffraction behavior for more customary wave motions. A determination of wave velocity (V_2) for second sound is obtainable from the observed Bragg angles. Results of an investigation on the propagation of second sound in rotating liquid helium are presented.

TABLE OF CONTENTS

FIGURES (APPENDIX II)

I. INTRODUCTION

Of all the curious properties of liquid helium below its transition temperature the most unusual and most illuminating is its ability to sustain a thermal wave. Temperature fluctuations introduced into the liquid propagate and preserve their form as characteristic of a general wave propagation, transporting energy and entropy with a definite velocity. This kind of thermal behavior, called second sound, is quite distinct from the usual diffusive flow of heat characteristic of most material and is unique to the form of helium existing below 2.186°K - liquid helium II. Above this transition temperature (called the λ-temperature) the liquid behaves in comparatively normal manner; but upon cooling below this temperature liquid helium alone is able to escape the consequences of the Nernst theorem which forces other matter to freeze. The combination of small interatomic forces along with a very large zero point motion, because of the magnitude of $\hbar/m$, allows helium to lose entropy in another fashion. The resulting behavior of helium on a macroscopic scale is thus a direct consequence of the ultimate quantum nature of matter.

Various theoretical models have been proposed to account for this behavior in helium. The first historically was that of F. London (1) who suggested that helium displays the phenomenon of condensation of Bose particles as predicted by Einstein (2). Tisza (3) amplified this idea, applied it to a specific model of helium, and succeeded in giving a theoretical account of many of the properties of helium. Landau (4) applied quantum hydrodynamics to a low energy system of particles apparently disregarding the effect of the particle statistics. The resulting excitation gas, composed of two types of fundamental excitations phonons and rotons, is taken as a model of liquid helium. Feynman (5) applied first principles to a low energy system of Bose particles, calculating the momentum-energy spectrum of the

system. This treatment directly yields many of the properties of liquid helium.

The one unifying feature of all the theoretical attempts at describing liquid helium is the result that the liquid is best described macroscopically as composed of two independent, non interacting momentum fields; one field containing all the entropy and viscosity of the liquid while the other has zero entropy and viscosity. This viewpoint allows the separating off of a degree of freedom of the system. Macroscopically there can now exist two types of longitudual oscillation - the pressure oscillations (sound waves) with both momentum fields in phase and entropy oscillations with the momentum fields out of phase. This second kind of oscillation is the second sound alluded to previously. From a study of its properties many of the characteristics of this quantum liquid can be found.

The existence of this kind of internal motion in the liquid was first determined by Peshkov (6) who experimentally investigated a resonant standing-wave system. The ability of second sound to proceed independently as a self-maintained thermal packet was determined by Pellam (7) who utilized the pulse method to investigate the transmission of thermal pulses and their subsequent multiple reflections.

The remaining property required for establishing second sound as satisfying unequivocally all the demands of the wave equation has been its ability to undergo diffraction in conformity to Huygens' principle. The purpose of this investigation has been to determine whether such diffraction is observable and, if so, whether the diffraction laws charactizing the more familiar forms of wave propagation are obeyed. This is at once the most demanding, yet the most conclusive, test to which the wave nature of second sound can be put.

II. METHOD AND EQUIPMENT

A) Method

The general procedure has been to excite second sound waves from a "thermal grating" consisting of a linear array of heater elements possessing a spatial periodicity and undergoing periodic in-phase heating. Interference effects would be expected to produce a primary (zero order) beam normal to the plane of the elements and sharply defined secondary beams at angles appropriate to constructive interference. The presence and location of such beams were investigated by means of a thermally sensitive receiver used to probe the surrounding thermal field.

B) Equipment

1) Thermal Grating

A "thermal grating" composed of a series of equally spaced, parallel, line sources constituted the heater array. This grating, shown in figure 1*, consisted of (30) thin parallel strips (G) of gold, spaced at an interval $\delta \cong 3/4$ mm. The gold strips were formed by vacuum evaporation through a screen onto the plane lucite surface (L). The elements are connected in parallel by the terminating electrodes (E) forming a resistance element, whose resistance of approximately 100 ohms is not a function of temperature in the liquid helium range. The elements of the resulting antenna array are heated in phase by applying an alternating voltage across the electrodes. Half of the power generated in the grating appears as a constant heat flow out of the experimental chamber through the holes (h) while the other half (with its frequency doubled) is available for second sound.

2) Detection System

In order to detect these thermal waves a sensitive, high frequency thermometer must be used. By the nature of the second

*Figures in section VIII (Appendix II)

sound it is necessary to measure the fluctuating temperature and not the time average - - the high thermal conductivity of helium keeps the time average temperature the same everywhere throughout the liquid. The thermometer used was a bolometer in conjunction with a tuned amplifier system. Established techniques (8) using a current carrying carbon film as the low inertia bolometer were employed. A rectangular receiver surface (roughly 3 mm x 20 mm) supporting uniform current density between electrodes on opposite edges measured the instantaneous temperature fluctuation averaged over its surface, and thus constituted a phase sensitive thermal detector. The phase sensitive nature of the detector allowed the detector to be placed close (28 mm) to the grating and still (by nature of its plane form) respond only to plane waves. Some deviation from this ideal behavior occurs because of interference effects resulting from the finite dimensions of the detector. For reasons to be discussed later, the response (S) for the present system is actually influenced in this respect only by the finite length (P) of the detector, for which the sensitivity pattern S (α) becomes

$$S = S_0 \frac{\left(\sin \frac{\pi P}{\lambda} \sin \alpha\right)}{\left(\frac{\pi P}{\lambda} \sin \alpha\right)}$$

for waves incident at angle (α) to the normal. From the form of the function S it is evident that the greatest response is to waves arriving within the angle $\alpha \simeq \lambda/P$. For the geometry used in this experiment $\alpha \simeq \lambda/P \simeq 1^{\circ}$, representing close enough approximation to the ideal behavior for the purposes of the experiment.

3) Experimental Chamber

A cut away section of the experimental chamber (machined from an initial 1 1/2 inch length of lucite tubing 2 1/2 inches in diameter) is shown with the top removed in figure 2.

The bolometer (B) is clamped securely to the brass stirrup (S) and can be rotated about a vertical axis (a-b). Two conical bearings at (a) and (b) maintain rigid alignment as the bolometer is rotated, scanning the thermal field. The bolometer is connected electrically to the amplifier system by coaxial cable; the input and output circuits are kept entirely separate in the liquid helium - - not even sharing a common ground.

Figure 3 gives a view of the complete low temperature unit. The mechanical connection of the stirrup to the external drive is through an expansion and universal joint (J) and the drive shaft (D). The drive shaft is aligned by tightly compressed glass wool surfaces (g), finally passing out of the dewar system through an O-ring seal (O) above which mechanical rigidity is assured by a ball bearing (A). An electric motor with a precision speed reduction gear arrangement provides external scanning drive. The sweep rate can be altered but was predominantly 7.2°/min in this experiment.

The antenna array (L) was aligned with its midpoint parallel to (a-b) (see figure 2) and served also to close the chamber, leaving direct connection with the external helium bath predominantly through the holes (h). All internal surfaces of the chamber and the stirrup (except the grating and the bolometer) were covered with felt to supress multiple reflections. It may be noted here that this geometry enables the study of a free wave, unhampered by standing wave effects except when grating and bolometer are parallel. The secondary reflections

are immediately removed from the direction of the beam under investigation and are absorbed.

4) Electronic

a) Source

An alternating current from a signal generator*) is supplied to the grating through a coaxial line. The second sound frequencies used in the experiment range from about 45 kilocycles $sec.^{-1}$ to 75 kilocycles $sec.^{-1}$. Because an alternating current generates heat twice each cycle these second sound frequencies are generated by a current at half frequency.

b) Amplifier

A block diagram of the amplifier system is shown in figure 4. The bolometer (R) is part of a simple LCR circuit (figure 5) with a Q of $\omega L/R$ and resonant angular frequency ω of $\omega = (LC_1)^{-\frac{1}{2}}$. $C_2 >> C_1$ is a blocking condenser and $r >> R$ serves to determine the direct current through R maintained for this experiment at about 1 milliampere. The Q obtainable is limited by R and by the available inductors but ranges in the neighborhood of 20. This circuit at once eliminates the troublesome subharmonic pickup present from the driving frequency and also multiplies the voltage appearing across R (because of bolometer action) by Q - - giving a virtually noise free gain of Q before entering the preamplifier.

The preamplifier is a tuned cascode amplifier**) which, when used with the tuned bolometer input, has a Q of about 60 and a gain of roughly 10^3. The output of the preamplifier is

---

*) Hewlett Packard, Model 200 CD.

**) Circuits are shown in Appendix II.

amplitude modulated by a mechanical chopper at 280 cycles $sec.^{-1}$. This chopped output feeds into a "pulse amplifier" and amplitude modulation detector whose output goes to a filter of 4 cycles $sec.^{-1}$ frequency width and adjustable time constant. The signal finally appears as a direct current measured either on a meter or recorded on a chart recorder. The overall gain is roughly 5×10^{5} with an equivalent input noise of 2×10^{-8} volts, and (for a one second time constant) noise fluctuations of 4×10^{-9} volts. The noise fluctuations of course limit the measurement sensitivity, but provide a simple non-zero background signal level. These fluctuations can be further reduced by increasing the time constant of the system (average over more cycles) but the practical limit is determined by how rapidly deliberate changes are to be made in the signal level.

With a power input of about 50 milliwatts to the helium the major beams give a maximum signal at the bolometer of about a micro volt, corresponding to a signal to noise fluctuation of about 250/1. This magnitude of signal involves a temperature fluctuation of the bolometer of about 5×10^{-6}°K.

III. ANALYSIS

The set of cylindrical wavelets produced by a plane array of many identical line sources, excited in phase, will combine in certain directions to form plane waves. This effect, well documented from multiple slit optics, presumably applies equally well to the thermal wave. The analytic expression for the amplitude ($R(\theta)$) of the plane wave produced in the direction θ by N line elements spaced at equal intervals (δ) is (9):

$$R(\theta) \propto \frac{\sin\left(\frac{N\pi\delta}{\lambda} \sin\theta\right)}{\sin\left(\frac{\pi\delta}{\lambda} \sin\theta\right)} \qquad (1)$$

The angle θ is determined by the direction of the plane wave (wavelength λ) with respect to the normal to the array.

The properties of function (1) are well known. From the form of this function it is evident that the maximum amplitude occurs at angles (θ) for which the condition

$$\delta \sin\theta = n\lambda , \qquad (n = \text{integer}) \qquad (2)$$

holds. This just states the requirement that the "thermal path" for adjacent sources differ by $n\lambda$. Only for this condition can the cylindrical wavelets combine to present a constant phase plane surface. For such maxima, the amplitude function (R) for the line source array becomes proportional to N, and just N times the contribution from an individual source.

There will similarly be zeros in the signal whenever there are equal numbers of oppositely phased contributions from individual line sources, i.e.

$$N\delta \sin\theta = m\lambda \qquad (m = \text{integer}) \qquad (3)$$

$(0<m<N)$. This represents the condition for which equal numbers of elements exist whose thermal paths differ by $\lambda/2$. Also the position of the first zero provides a criterion for expressing the effective "beam width" ($\triangle$) of the "straight-ahead" beam (n = 0):

$$\triangle \simeq \sin\theta = \lambda/N\delta \tag{4}$$

Similar criteria express the "beam width" ($\triangle$) for the secondary beams (for $|n|>0$)

$$\triangle \simeq \lambda/N\delta\cos\theta \tag{5a}$$

where the array becomes effectively foreshortened to its projected length $N\delta\cos\theta$. We see from the form of (2) and (5a) that the angular position of the major beam is determined by λ/δ, while the "beam width" ($\triangle$) for this position is determined by $1/N$, as $\theta \simeq \lambda/N\delta$.

It turns out to be convenient to put $\triangle$ in a form containing only geometric factors. Eliminating λ/δ from equations (2), and (5a), the halfwidth ($\triangle$) becomes

$$\triangle = \frac{1}{nN}\tan\theta \tag{5b}$$

for which the actual frequency dependence of $\triangle$ appears only in the angular position of the beam.

From the form of (1) it also follows that between the major peaks there falls a sequence of "sub-peaks" produced by conditions of partial reinforcement, and located at angles (θ) for which

$$N\delta\sin\theta = m\lambda \qquad (m = \text{half-integer} > \tfrac{1}{2}) \tag{6}$$

Formation of such sub-peaks may be visualized easily on the basis of mutual cancellation of some fraction of the available source elements. For example, when

$$(N\delta/3)\sin\theta = \lambda/2 \qquad (7)$$

($m = 3/2$ in (6)) two-thirds of the sources mutually cancel, leaving the remaining one-third to form a signal by phase addition, for which the phase span is π. Adding these on the "vibration curve" principle, the amplitude $R(\theta)_{sub\text{-}peak}$ may be evaluated

$$R(\theta)_{sub\text{-}peak} \propto \frac{2}{\pi}\left(\frac{N}{3}\right) \qquad (8)$$

with similar arguments holding for each half-integer value of (m) greater than one half. By either method, the amplitudes of such sub-peaks falling between the major beams become

$$R(\theta)_{sub\text{-}peak} \propto \frac{(-1)^{(m-\frac{1}{2})}}{\sin(m\pi/N)} \simeq \frac{(-1)^{m-\frac{1}{2}}}{\pi}\left(\frac{N}{m}\right);\ (m/N)<<1 \qquad (9)$$

$$(m = \text{half-integer} > \tfrac{1}{2})$$

Figure 6, showing the distribution of amplitudes, was constructed from the expression of equation (9) (for the particular case of $N = 30$). A series of N-2 alternate phase sub-peaks occurs, reaching minimum magnitude midway between the major peaks where the heights are down by a factor (1/N). Besides providing signal distribution among sub-peaks, the behavior shown in figure 6 near the major beams represents the fine-structure observed experimentally in their vicinity. Such structure will be discussed more fully under (IV) Experimental Results, where the effects of other aspects of the pattern will be pointed out.

Having dwelt on the details adjacent to the main beams, the overall features of the pattern must be considered. Clearly, if equation (1)

fully represented the behavior, all major peaks (when m = N) would possess equal amplitude (proportional to N in each case). The situation is complicated, however, by the further fact that the elements have an actual width (w). Accordingly, instead of radiating symmetrically, as from the line elements assumed for 1, each element itself possesses a wave radiation amplitude pattern given by

$$R(\theta)_{\text{elem.}} \propto \frac{\sin\left[\left(\frac{\pi w}{\lambda}\right)\sin\theta\right]}{\left[\left(\frac{\pi w}{\lambda}\right)\sin\theta\right]} \tag{10}$$

As a result expression (1) for pure line elements is "modulated" by this factor, so that the overall radiation pattern becomes

$$R(\theta) \propto \frac{\sin\left[\left(\frac{\pi w}{\lambda}\right)\sin\theta\right]}{\left[\left(\frac{\pi w}{\lambda}\right)\sin\theta\right]} \; \frac{\sin\left[\left(\frac{N\pi\delta}{\lambda}\right)\sin\theta\right]}{\sin\left[\left(\frac{\pi\delta}{\lambda}\right)\sin\theta\right]} \tag{11}$$

or, for simplicity

$$R(\theta) \propto \frac{\sin\beta}{\beta} \; \frac{\sin N\phi}{\sin\phi} \tag{12}$$

where $\beta = \frac{\pi w}{\lambda}\sin\theta$, and $\phi = \frac{\pi\delta}{\lambda}\sin\theta$.

The general expression for the wave amplitude (12) simplifies considerably for the major beams. As was shown in equation (2) the major beam peaks occur whenever $\delta\sin\theta = n\lambda$. Under this condition equation (12) reduces to

$$R(\theta)_{\text{max.}} \propto (-1)^{(N-1)n} \; N\frac{\sin\beta_n}{\beta_n} \quad *) \tag{13}$$

with $\beta_n = \frac{n\pi w}{\delta}$. The relative amplitudes of the major beams are thus

*) The even number beams (n = even integer) are always of positive phase, while the phase of the odd number beams depends on the number of elements (N).

determined only by geometric factors involving the array itself and are independent of wave length! This effect will be illustrated in the experimental data.

Thus far the derivation has concerned only the wave generating characteristics of the grating array, and remains strictly valid, therefore, only for a plane receiver surface of infinite extent. Actually, the finite dimensions of the actual experimental detector introduce still further modifying effects. Specifically, the sensitivity of the receiver element itself depends upon the angle of incidence (α) (measured from the normal to the detection surface) at which the wave arrives. This sensitivity pattern $S(\alpha)$,

$$S(\alpha) = S_o \frac{\sin \gamma}{\gamma} \qquad \gamma = \left(\frac{\pi P}{\lambda}\right) \sin \alpha \tag{14}$$

where (P) is the detector surface length, results in the detector having a very slight "peripheral vision", i.e. being able to detect strong signals at other than normal incidence. Since the beams are not spatially separated near the grating, the detector is actually "illuminated" by a complicated array of superposed simultaneously arriving beams and sub-beams, approaching from a variety of propagation directions.

The gross radiation pattern measured will certainly represent predominantly the detection of waves striking the receiver surface at normal incidence, and the major peaks themselves will undergo but slight modification. However, the detailed fine structure accompanying the major peaks, and particularly the relatively low intensity sub-peak array, can be profoundly modified by the effects of receiver "peripheral vision", as will become evident from the experimental results.

IV. EXPERIMENTAL RESULTS

Chart recordings of the experimental results are shown in figures 7, where signal amplitude (arbitrary units) is recorded versus angle (θ) (degrees). Data are shown for two frequencies (46.4 kilocycles $sec.^{-1}$ and 72.6 kilocycles $sec.^{-1}$) and at each frequency recordings are shown for three temperatures. The data unmistakably show the expected major interference effects displaying beams out to n = 4 at the higher temperatures.

The details of the major beams and the nearby subpeaks conform well to the behavior expected from the preceding analysis. The predicted value for the halfwidth $(\triangle)_{deg}$ (equation 5b), expressed in angular degrees, reduces to

$$(\triangle)_{deg} \simeq \frac{2}{n} \tan \theta \qquad (15)$$

for the special case N = 30. The experimental results agree quite well with this formula. For example, from figure 7a $\triangle$ is measured to be 0.54° for the n = 3 beam while calculation using the corresponding observed value of θ gives 0.45°. Similarly, the n = 1 beam from figure 7f has a measured $\triangle = 0.95^{\circ}$ and a calculated value of $\triangle = 0.77^{\circ}$. As expected from figure 6 the major beams are seen (figures 7) to have approximately twice the width of the close-by minor peaks.

The calculated relative intensity of the major beams (equation 13) agrees only moderately well with experimental measurements. For the grating used in these experiments $\delta \simeq 3/4$ millimeter and $w \simeq 1/4$ millimeter. Rewriting equation 10 neglecting the sign of the phase the wave amplitude becomes:

$$R(\theta) \propto N \frac{\sin \beta_n}{\beta_n} \qquad (16)$$

with $\beta_n \simeq \frac{n\pi}{3}$. As an example of experimental confirmation, data from figure 7a are presented normalized to $R_{n=1}(\theta)$.

n	R_n/R_1 (calc.)	R_n/R_1 (exp.)
1	1.0	1.0
2	.5	.65
3	0	.15
4	.25	.02

These results will be considered again in section (V) Discussion.

The second sound velocity (V_2) can be calculated using equation 2. Assuming no dispersion the wave length (λ) is simply related to the frequency (ν), and equation 2 becomes:

$$V_2 = \frac{\nu\,\delta}{n} \sin\theta \qquad (17)$$

Accurate relative velocity measurements then simply involve measurement of the angle θ. Velocity as a function of temperature measured in this manner is presented in figure 8 for a number of frequencies (ν). The resulting velocities are in good agreement with measurements by other techniques (10) and constitute the first direct measure of the velocity of a free second sound wave of definite frequency. To within the point scatter (1 percent maximum) there is no dispersion in the frequency range investigated. The high precision possible with this technique was not attempted being limited here mainly by considerations of temperature measurement.

With decreasing temperature the absolute amplitude of the signal is seen to increase, figures 7, raising the expected subpeaks above the noise level. The change in absolute signal amplitude with temperature is governed mainly by the specific heat (C). For a given heat input (ΔQ) the initial temperature fluctuation (ΔT) is $T = \frac{1}{C}\Delta Q$.

In this case the ΔT propagates as an attenuated wave according to $\Delta T \propto \frac{e^{-\alpha x}}{C} \Delta Q$, where α is an amplitude attenuation coefficient ($cm.^{-1}$) expressing the rate of decay with distance (x) (cm.). For a constant power input the amplitude of the second sound signal will be a measure of the quantity $\frac{e^{-\alpha x}}{C}$ averaged over the detector surface. This function (using previously determined values of α (8) and C (11) is plotted in figure 9 normalized to the accompanying experimental points at $1.95^{\circ}K$ where the attenuation is minimum. The experimental internal consistency among these various parameters is evident from figure 9. For the frequencies and geometry used, the effects of attenuation in the helium actually proved unimportant except at the highest and lowest temperatures.

V. DISCUSSION

The experimental results conclusively demonstrate the true wave nature of second sound. Overall features of the interference patterns produced by a thermal grating conform well to the behavior predicted by an application of Huygens' principle (equation 12). The ideal detailed substructure, however, is somewhat masked by the effects of a detector of finite length*). The detector sensitivity pattern (equation 14) is of the familiar form

$$S(\alpha) = S_o \frac{\sin\gamma}{\gamma} \quad \gamma = \frac{\pi P}{\lambda} \sin\alpha$$

where for this experiment $P \simeq 20$ mm or 60λ. The first zero of the sensitivity pattern thus falls at $\alpha \simeq 1^\circ$. The primary result of the finite length, then, is to give the detector a roughly 2° "field of vision".

Clearly, the existence of a first zero signal adjacent to the major peaks, required by equation 12 for normal incidence, will be modified by the remnant signals from the dominant peak arriving at angles slightly off normal but for which sensitivity exists. This effect keeps the first minima from being actually zero and shifts the minimum away from the main beam (as observed experimentally).

Aside from the primary effect of producing an immediate field of vision about the normal, the finite length of the detector also allows feeble detection of waves at relatively large angle (α). The pattern detected in the region between the major beams of the transmitter can be influenced by these major beams themselves. In fact the complicated response to the large amplitude waves at non-normal incidence evidently effectively overpower the low level wave

*) The comparatively narrow width of the detector can influence only the signal level, but not the radiation pattern of interest to the present experiment. The detector width does not affect the pattern shape in a plane perpendicular to the source elements.

normal to the surface. The delicate substructure is thus completely masked by a combination of factors - - the integrating effect of the finite field of vision and the response to large amplitude beams at non-normal incidence.

The effect of the finite width of the source element appears in the relative amplitudes of the major beams (equation 13). It had been hoped to verify this effect dramatically by showing complete absence of the $n = 3$ beam (see (IV) Experimental Results). That is, for the experimental geometry used ($\delta/w = 3$) the radiation in the direction of the $n = 3$ should have vanished completely. As noted in section (IV) Experimental Results this did not occur. Presumably, the homogeneity of the individual grating element was not sufficient to allow perfect cancellation.

Regardless of these higher order deviations, the overall results are considered to correspond very well with predictions. In fact, better than anticipated, as original intentions were merely to observe the presence of secondary beams, with no expectation, for example, of observing fine structure of such beams.

VI. CONCLUSION

The true wave nature of second sound has been verified in detail by an investigation of the heat beams surrounding a thermal grating. Many orders of interference are observed for these highly collimated beams, corresponding exactly to effects expected from Huygens' principle applied to a true wave motion. This may be regarded as the most demanding and conclusive test to which thermal waves in liquid helium II have been subjected.

VII. APPENDIX I

INVESTIGATIONS IN ROTATING LIQUID HELIUM II

Introduction:

The existence of a superfluid component of zero viscosity in liquid helium II raises interesting questions as to the nature and indeed, the existence of rotation (or circulation) in superfluid helium. Experiments on the gross properties of the liquid helium II such as the shape of the free surface (12) or the angular momentum of the rotating liquid (13) give results expected from classical physics. However experiments at very low rotation rates (14) or experiments designed to investigate rotating helium on a more microscopic scale (15) indicate deviations from the classical behavior.

Feynman (5) has considered the problem of rotating liquid helium at absolute zero temperature concluding from first principles (and verifying an independent suggestion of Onsager (16))that rotating superfluid helium should contain quantized vortex lines. The density of these lines depends on the macroscopic rotation rate (Ω) and the atomic constants - - mass (m) of the helium atom and Planck's constant (h). This density of $\frac{2m\Omega}{h} = (2.1 \times 10^3 \Omega)(cm.^{-2})$, at moderate rotation rate (Ω)(rad.sec.$^{-1}$) gives the system the gross appearance of a classical rotation while deviation from classical motion can be expected to occur in an investigation on a scale comparable to the spacing between lines.

Method:

Sharply defined second sound beams from a grating array, uninfluenced by standing wave effects, were suggested by Professor Feynman to be a probe of the helium on a scale of the wave length (λ). For a wave length of 1/3 millimeter (roughly that used in this experiment)

the wavelength equals the spacing of the vortex lines at a rotation rate of about 4 revolutions $min.^{-1}$. Consequently it was suggested that an experimental investigation be undertaken to examine the propagation of second sound in rotating liquid helium, particularly in the region where the vortex line spacing approximates the wavelength. Measurements were undertaken to determine the effect of rotation on second sound attenuation, on the gross features of the diffraction pattern (introduction of additional beams by cooperative scattering of second sound by ordered vortex lines), and on the angular position of the second sound beams.

Equipment and Technique:

The entire dewar system and vacuum line, along with some of the electronic equipment were mounted on a platform (figure 10) which could be rotated in either direction about a vertical axis at a constant rate from about one to one hundred revolutions $min.^{-1}$. The vacuum line (V) joins to the laboratory vacuum system through a rotating vacuum joint (J) comprised of a double O-ring seal. The servo-motor (M) serves to adjust the angular position of the bolometer through a gear reduction arrangement while the system is in rotation. Control signals for the servo-motor as well as sixty-cycle power for the system enter through the mercury pools (H). Higher frequency power for second sound generation enters through the shielded mercury pools (h), while the output signal leaves the rotating system through the co-axial transformer (T) after amplification and modulation by the electronics (E).

The measurement technique for measuring small differences in the second sound signal employs the same equipment as described previously with the addition of a comparison signal derived from the input to the helium which serves both to reduce the effect of fluctuations in the input power and to increase the sensitivity to amplitude changes of the second sound. Figure 11 shows a block

diagram of the equipment where the dotted line encloses the rotatable equipment.

The two signals (one from the helium, the other from the frequency doubler) are set to slightly different amplitudes; resulting (by the action of the chopper) in an amplitude modulation at 280 cycles $sec.^{-1}$ of the carrier frequency (ν). The modulated carrier frequency leaves the rotating system through the co-axial transformer (T), is amplified again and the modulation signal at 280 cycles filtered through a bandwidth of ± 2 cycles $sec.^{-1}$, finally to be displayed as a chart recording and meter deflection.

With the comparison signal removed a typical order of magnitude for the n = 1 peak is 500 millivolts output signal with a fluctuation of $\pm$ 2 millivolts. The comparison signal is normally set about ten percent higher than the second sound signal, leaving roughly 50 millivolt difference signal. Thus a five percent change in the difference signal corresponds to a one half percent change in the second sound amplitude.

The electronic equipment was carefully tested to assure that the gain, stability, and noise level were unaffected by rotation. Mechanical stability of the experimental chamber, particularly the bolometer mounting, was carefully considered and tested to assure against possible spurious effects due to a mechanical misalignment under rotation.

Effect of Rotation on Second Sound Attenuation:

Attenuation measurements involve determining the change in second sound signal amplitude upon rotation of the helium. The first order beam (n = 1) was usually chosen for investigation, being the beam of greatest intensity without standing wave effects. Measurements of the amplitude change are made using the comparison signal and the partial compensation method mentioned previously.

In an actual measurement the bolometer is swept back and forth through the peak about four times per minute and readings taken at the second sound maximum. This is done to assure that signal amplitude changes are not the result of a position shift of the beam. Data are taken in five minute periods alternating standing still and rotating. In this way long term drifts in the equipment can be recognized and compensated.

The equipment is brought to a final steady angular velocity in roughly 5 seconds starting or stopping; however the effects of the initial turbulence in the helium decay in about 30 seconds. After the decay in the initial turbulent state there is no detectable change in the new signal level over periods up to 15 minutes (the longest interval measured).

The results of this investigation are inconclusive. The effect of rotation on the signal amplitude is small, being generally less than one percent up to 50 revolutions $min.^{-1}$, but detectable. However the observed effect is much more complicated than a simple attenuation, being a function of rotation direction, and indeed producing detailed changes in the diffraction pattern generally. Investigation of the first minima in the second sound intensity on either side of the n = 1 beam showed one minimum increased while the other decreased. Within the accuracy of the second sound diffraction pattern recordings (about 2 percent) there is no indication of additional beams being produced by rotation.

Effect of Rotation on Angular Position of Beams:

The sharpness of the second sound beams, as displayed in figures 7, suggests determining the change in beam direction by fixing the angular position of the detector to the steep side of a beam. A slight change in angular position of the beam then causes a relatively large change (δA) in signal amplitude by virtue of the

large value of the slope of the amplitude (A) curve $\partial A/\partial\theta \simeq 300\ \frac{mv}{\theta\sigma}$ (see figure 12). An easily detectable change of 10 millivolts thus corresponds to an angular shift of roughly .03 degree. Changing the fixed position of the bolometer from one side of a beam to the other reverses the sign of the amplitude change for a given shift. For example a shift toward increasing θ will increase the signal if the detector is fixed on the "outside" ($\theta > \theta_{n=1}$) of the beam and will decrease the signal if fixed on the "inside" ($\theta < \theta_{n=1}$) of the beam. Such spurious effects as noise generated by rotation, a symmetric beam shape change, or attenuation effects can be eliminated by taking data on both sides of a beam.

The experimental results again show a dependence on rotation sense. Data taken for a clockwise rotation (as seen looking down on the experimental chamber (figure 2) are consistent and show no dependence on second sound power level; however data taken for the counter-clockwise rotation direction are dependent on the power level although still reproducible.

The variations (δA) in amplitude observed on the steep slope of a peak are best expressed in terms of the ratio $(\delta A/A_1)$* where A_1 is the undisturbed overall height of the (n = 1) peak. The variations (δA) are observed at a position of roughly two-thirds maximum amplitude. The reasons for this criterion will be given shortly. Also for reasons to become apparent later, the ratio $(\delta A/A_1)$ is plotted (figure 13) as a function of the product $(\omega\Omega)$ where ω is the second sound angular frequency and Ω the rotation rate (radians $sec.^{-1}$).

---

*The quantity $\frac{\delta A}{A_n}$ can be formally related to a velocity change using $\frac{\delta A}{A_n} = \frac{1}{A_n}\frac{\partial A_n}{\partial\theta}\delta\theta$ where $\frac{\partial A_n}{\partial\theta} \simeq \frac{A}{\Delta} = \frac{AN\delta}{\lambda}\cos\theta$. Differentiating equation 2, the relation between velocity change δV_2 and a peakshift $\delta\theta$ is $\delta\theta = \frac{n\lambda}{(\cos\theta)\delta}\frac{\delta V_2}{V_2}$. Combining these results $\frac{\delta A}{A_n} = nN\frac{\delta V_2}{V_2}$.

Data from both sides of the peak show the same general effect -- a linear increase in $\delta A/A$, with $\omega\Omega$ until $\delta A/A$ "saturates", followed by comparative independence of $\delta A/A$ with further increase in $(\omega\Omega)$.

A sample of the raw data (chart recording) is shown (figure 14) for $\omega\Omega = 6 \times 10^5$ (sec.^{-2}), $\nu = 46.4$ kilocycles sec.^{-1} to illustrate the basic experimental measurements.

Close inspection of these data reveals a random fluctuation in signal height (with 20 - 30 sec. "period"), which furthermore proceeds to decrease upon rotation. This is generally true for all the data above $\Omega\omega \simeq 5 \times 10^5$ sec.^{-2}; the region in which $\frac{\delta A}{A_1}$ is roughly independent of Ω for fixed ω. Such behavior is consistent with the leveling off of $(\delta A/A_1)$ for large $\omega\Omega$, if the variations are attributable to fluctuations in the beam position. This assumption is further confirmed by the observation that no such fluctuations occur for the peak height at any rotation rate, the signal possessing only constant back-ground noise arising from known electronic sources. Similarly, for high rotation rates $(\omega\Omega \gtrsim 5 \times 10^5)$ the same electronic noise level remains after the signal fluctuations in $\delta A/A_1$ have been suppressed. Fluctuations in signal level are largely independent of rotation rate for rates lower than $\Omega\omega \simeq 5 \times 10^5$ (sec.^{-2}). This behavior suggests a kind of saturation occurs which limits both the fluctuation of the beam position and also its displacement under rotation.

Experimental quantities, peak amplitude (A_1) and amplitude change (δA), can easily be related to an angular shift, knowing the slope of the peak. Using the conversion factor*, $\delta\theta = (nN \cot\theta)^{-1} \frac{\delta A}{A}$, the

*The approximation to the slope $\frac{\delta A}{\partial\theta} \simeq \frac{A_1}{\Delta} = \frac{A_1 N\delta}{\lambda} \cos\theta$ is a good approximation to the slope near two-thirds amplitude and provides a simple analytic expression for it. For this reason the data were always taken at the two-thirds A_1 position. Thus $\frac{\delta A}{A_1} \simeq \frac{1}{A_1} \frac{\partial A}{\partial\theta} \delta\theta = \left(\frac{N\delta \cos\theta}{\lambda}\right)\delta\theta$ $= (nN \cot\theta)\, \delta\theta$.

data of figure 13 for $\theta > \theta_1$ are plotted as $\delta\theta$ versus Ω in figure 15. This presentation does not have the consistency evident in figure 13, but nevertheless shows a semi-universal behavior of $\delta\theta$ with Ω for low Ω. However the saturation now occurs at different values of Ω and $\delta\theta$ for each second sound angular frequency (ω).

This illustrates the choice of ($\omega\Omega$) as the only combination of independent parameters from which self-consistent results are attainable. Attempts to express experimental results in terms either of ω or Ω separately produced no consistent pattern (see figure 15). Only by combining the two in the form ($\omega\Omega$) as an independent parameter, could the results be reduced to a consistent pattern, or "universal curve".

The physical significance of the consistency displayed by the data in terms of the combination of parameters $\left(\frac{\delta A}{A_1}, \omega\Omega\right)$ is, at present, unknown. It appears doubtful (see figure 15) that a simple angular displacement of the beam in the rotating system is responsible for the effects. Likewise a small relative rotation between the two fluids seems unlikely as analysis based on this assumption leads to a frequency independent effect. The footnote on page 23 suggests that these effects could result from the velocity of second sound (V_2) in a rotating system being a function of $\omega\Omega$. In this event the maximum measured change in V_2 is on the order of one part in 10^3. It should be emphasized that aside from normalizing the data the only present justification for using the parameter ($\delta A/A_1$) is the resulting consistency of results.

A number of confirmatory experiments have been performed in an attempt to clarify the situation.

The possibility that these effects were due to a temperature change upon rotation which altered the second sound velocity (see figure 8) was excluded by finding the same kind of effect at $1.65^{\circ}K$ where the

slope of the velocity versus temperature curve is zero. Beam deflection measurements at 1.9°K, 1.65°K, 1.4°K, 1.25°K show the effect to be temperature dependent, the effect increasing monotonically with decreasing temperature.

The interaction of a heat flow with the second sound beam was investigated by making drastic changes in the heat flow path from the chamber to the helium bath. These modifications had no effect on measurements of the beam deflection taken under clockwise rotation but had a profound effect on those taken under counter-clockwise rotation. The counter-clockwise data are known from the other measurements to be a function of power level.

A second chamber was constructed with grating and bolometer in fixed positions to exclude any possibility of relative mechanical motion. Beam position in this case was varied by adjusting the temperature. Again, this precaution had no effect on the data taken under clockwise rotation. This chamber was inverted, yielding an interchange of the previous results with respect to rotation sense (clockwise became counter-clockwise and vice versa) indicating a geometry dependence complicating the results. The grating itself was inverted (to look at the other n = 1 beam) with no essential change in the effects due to rotation.

Conclusion:

No explanation for these results has been found. Beam position measurements taken for counter-clockwise rotation are complicated by heat currents while those taken for clockwise rotation seem free of this complexity. The results for the clockwise rotation can be displayed in a remarkably consistent fashion (figure 13) but are not understood at present in terms of the vortex line or any other model.

APPENDIX II

F I G U R E S

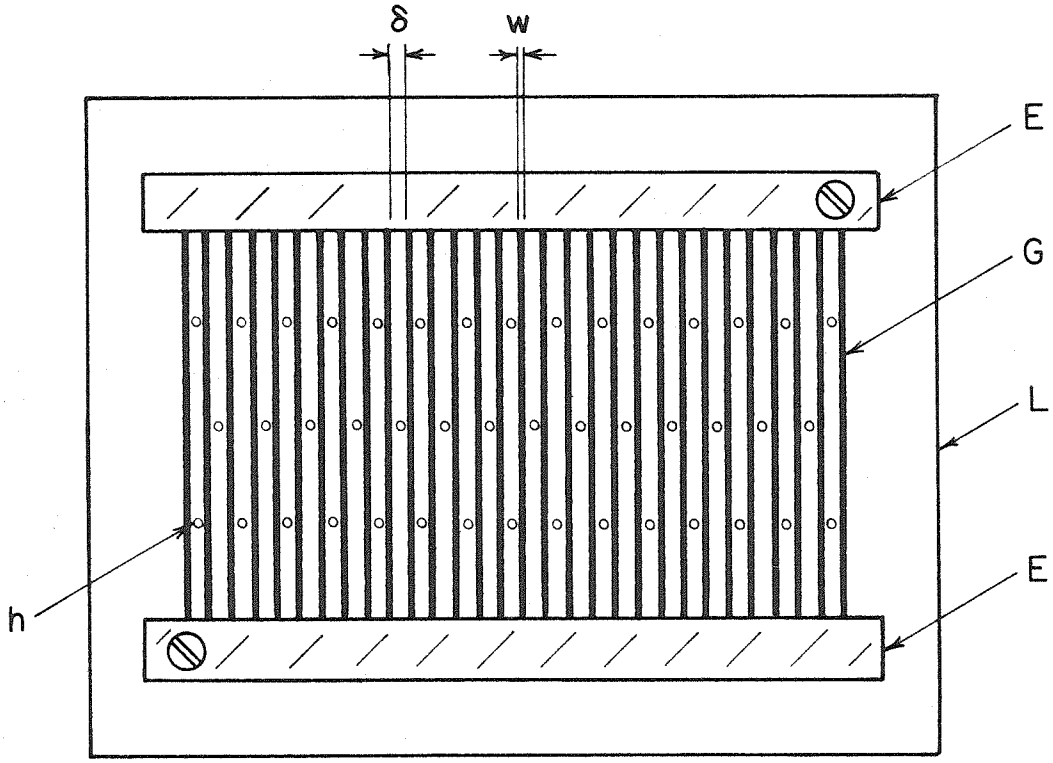

SECOND SOUND GRATING

Fig. 1

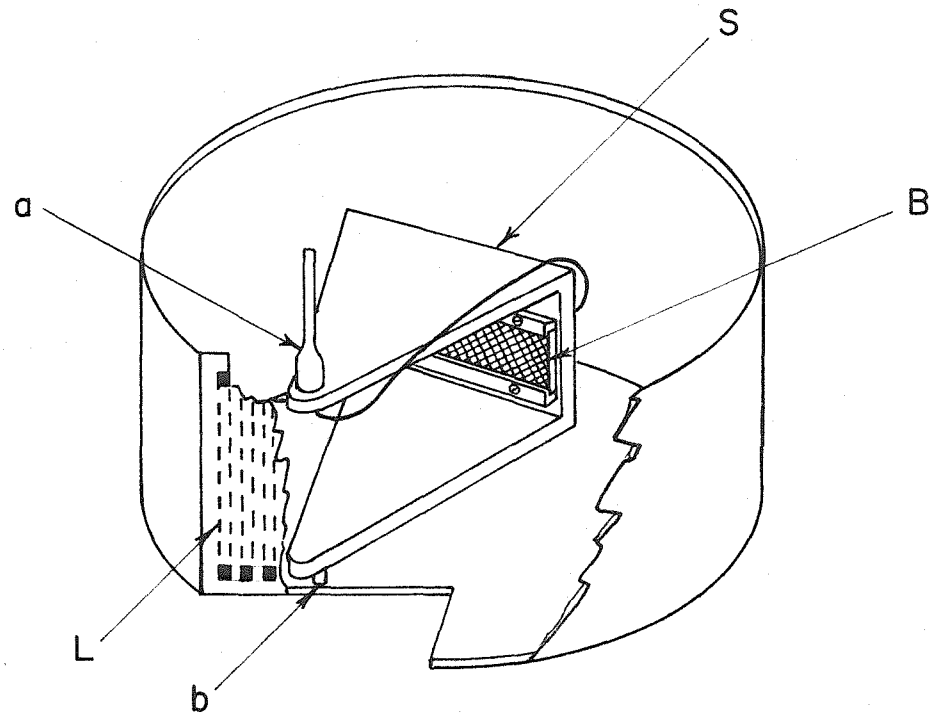

CUT-AWAY VIEW OF EXPERIMENTAL CHAMBER WITH TOP REMOVED

B - BOLOMETER

L - GRATING

S - BRASS "STIRRUP"

a, b - BEARINGS

EXPERIMENTAL CHAMBER

Fig. 2

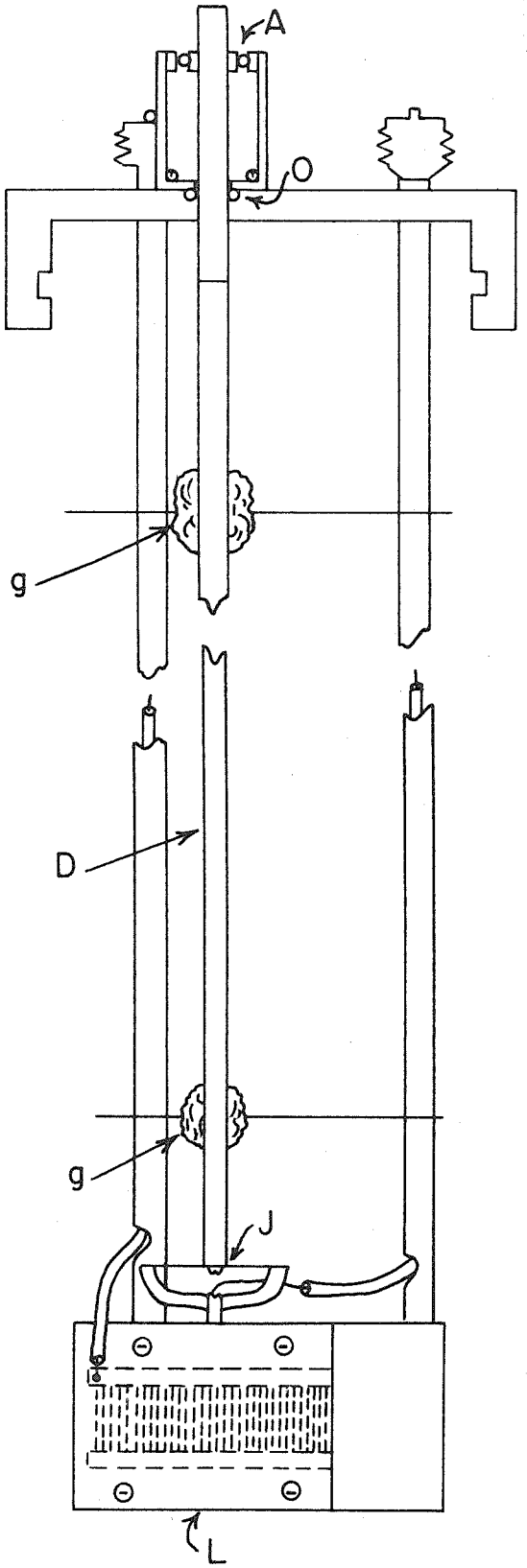

LOW TEMPERATURE UNIT

Figure 3

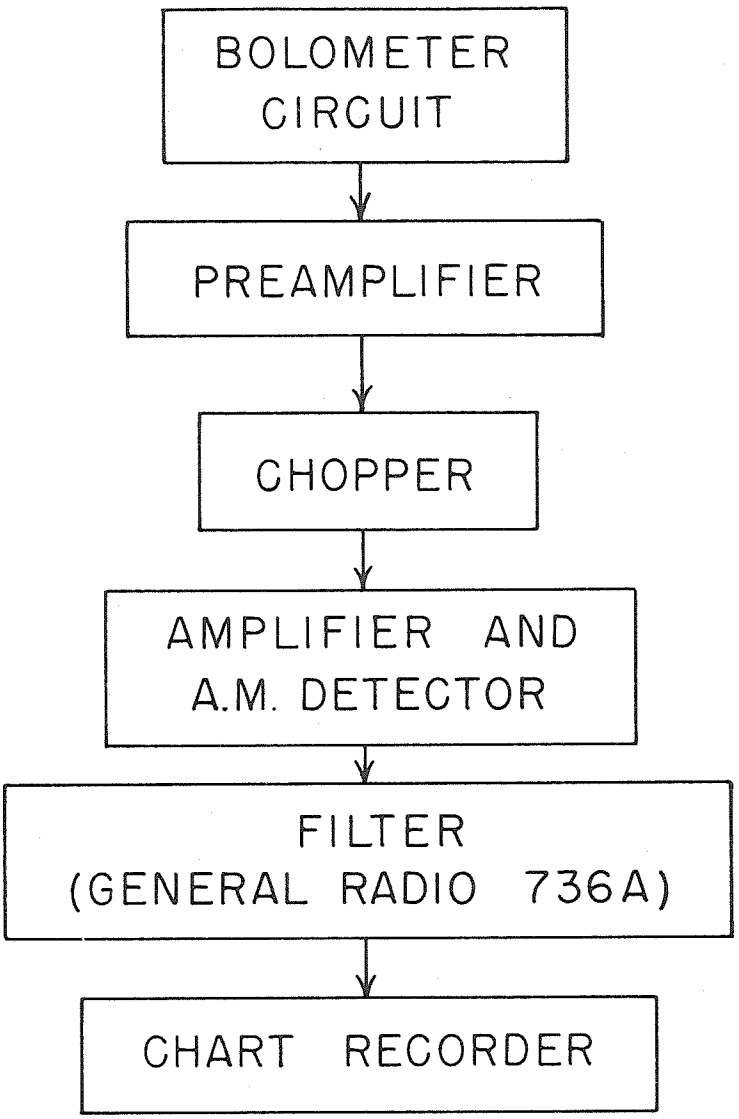

BLOCK DIAGRAM OF AMPLIFIER SYSTEM

Figure 4

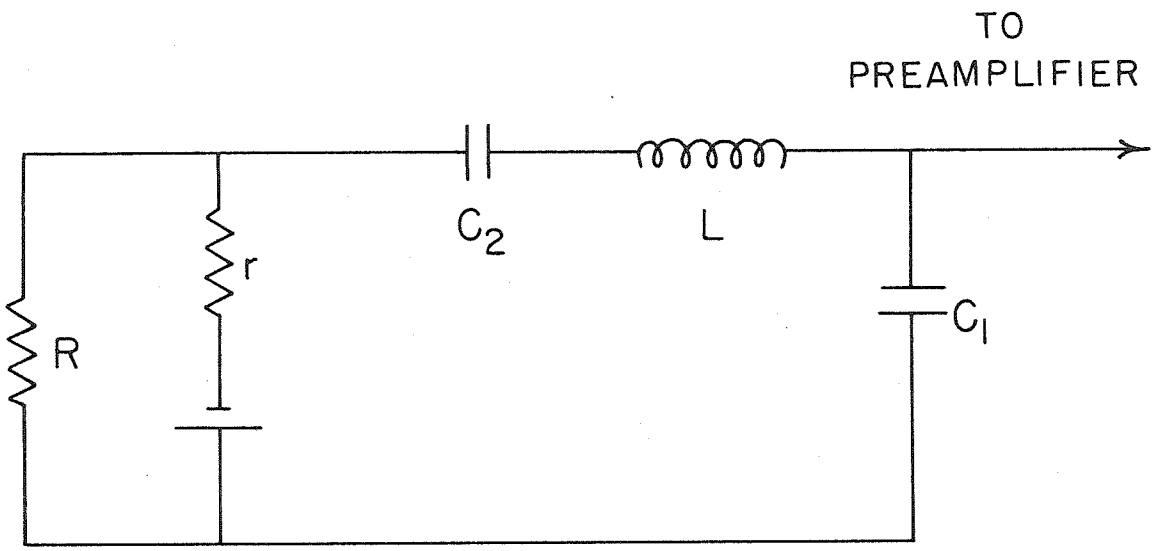

BOLOMETER CIRCUIT

Figure 5

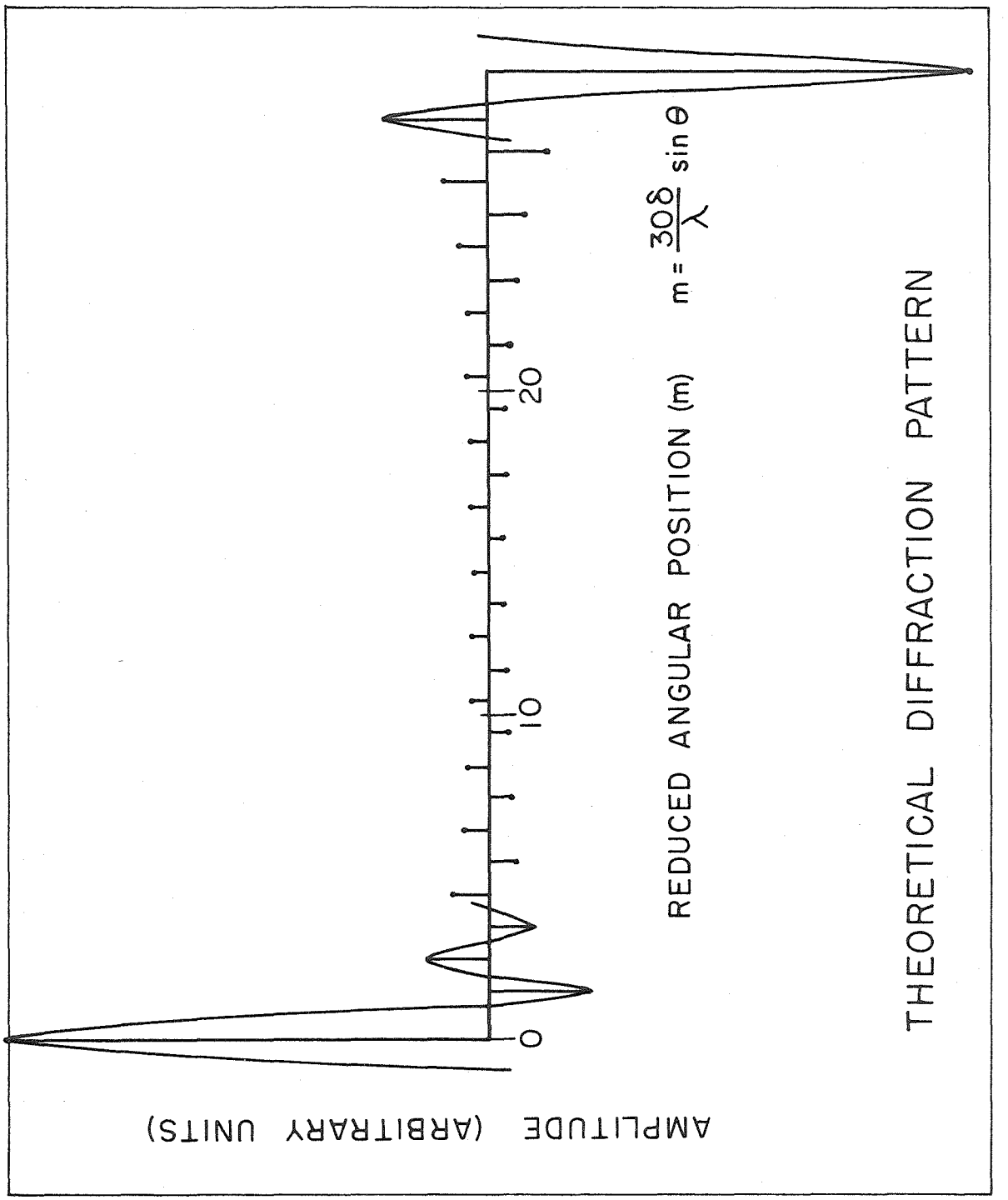
THEORETICAL DIFFRACTION PATTERN
$m = \frac{30\delta}{\lambda} \sin\theta$
REDUCED ANGULAR POSITION (m)
0
10
20
AMPLITUDE (ARBITRARY UNITS)

Figure 6

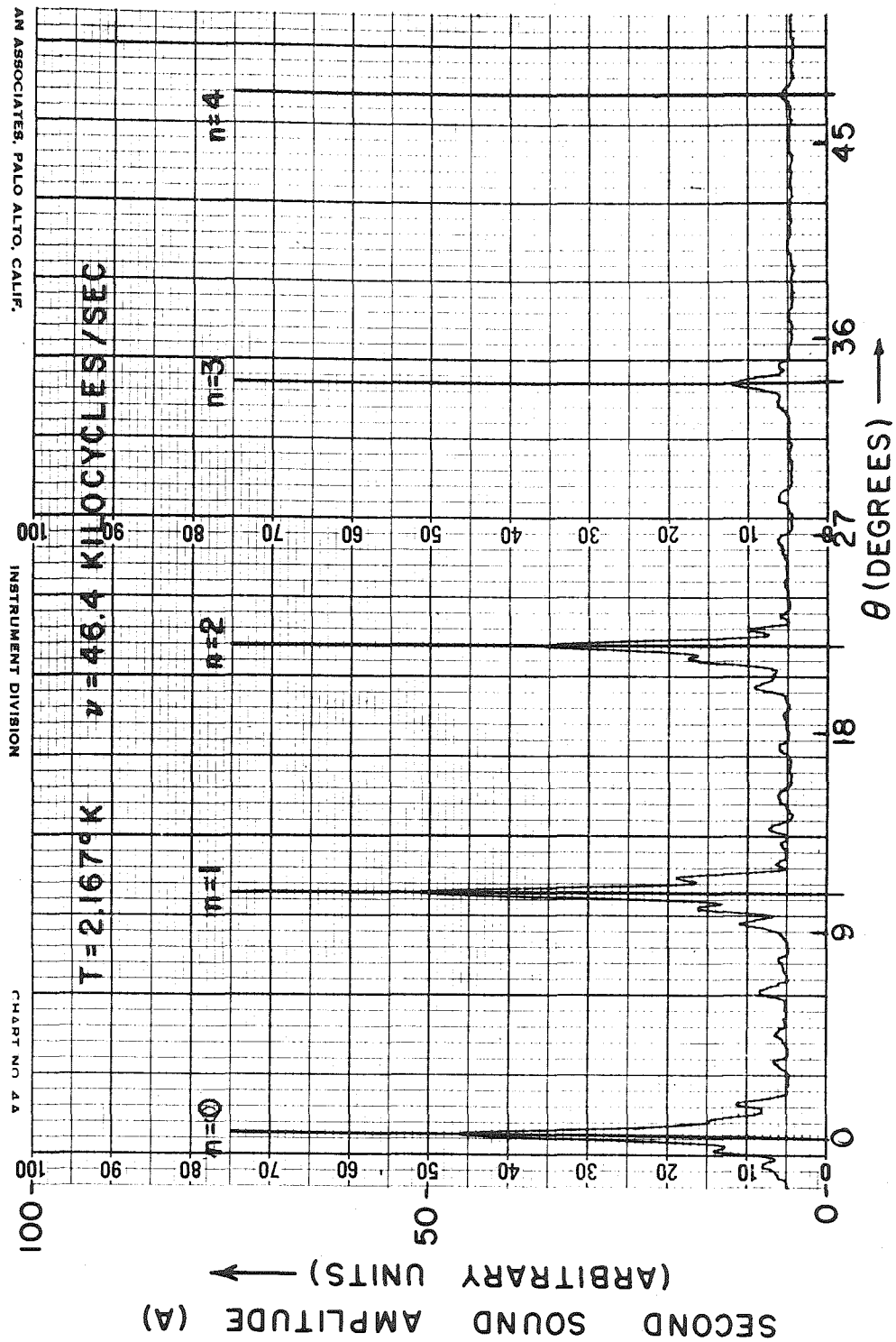

EXPERIMENTAL SECOND SOUND DIFFRACTION PATTERN

Figure 7(a)

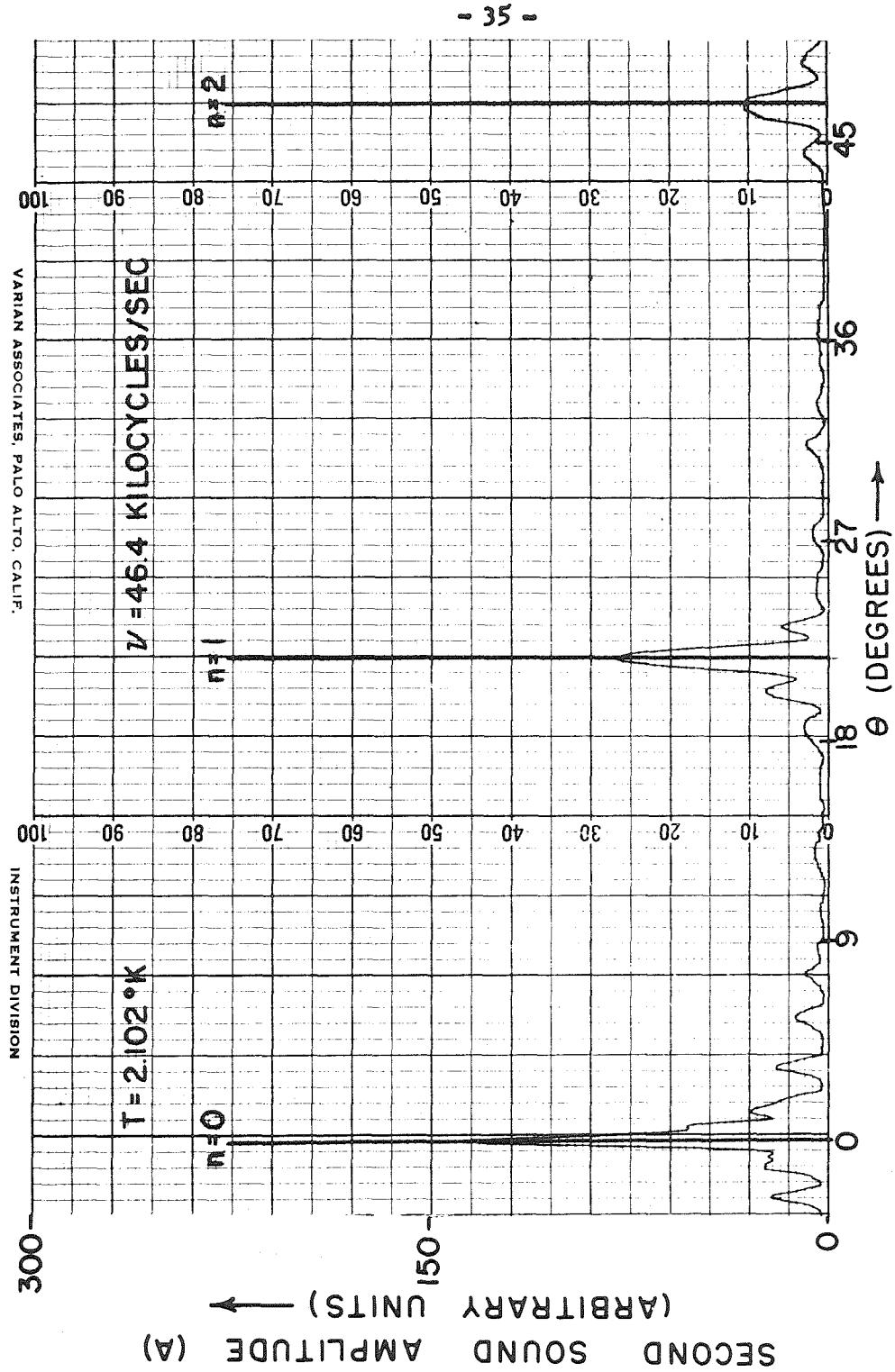

EXPERIMENTAL SECOND SOUND DIFFRACTION PATTERN

Figure 7(b)

EXPERIMENTAL SECOND SOUND DIFFRACTION PATTERN
SECOND SOUND AMPLITUDE (A)
(ARBITRARY UNITS)
1000
500
0
T = 1.404 °K
ν = 46.4 KILOCYCLES/SEC
n = 0
n = 1
0
10
20
30
40
50
60
70
80
90
100
0
9
18
27
36
45
θ (DEGREES)

Figure 7(c)

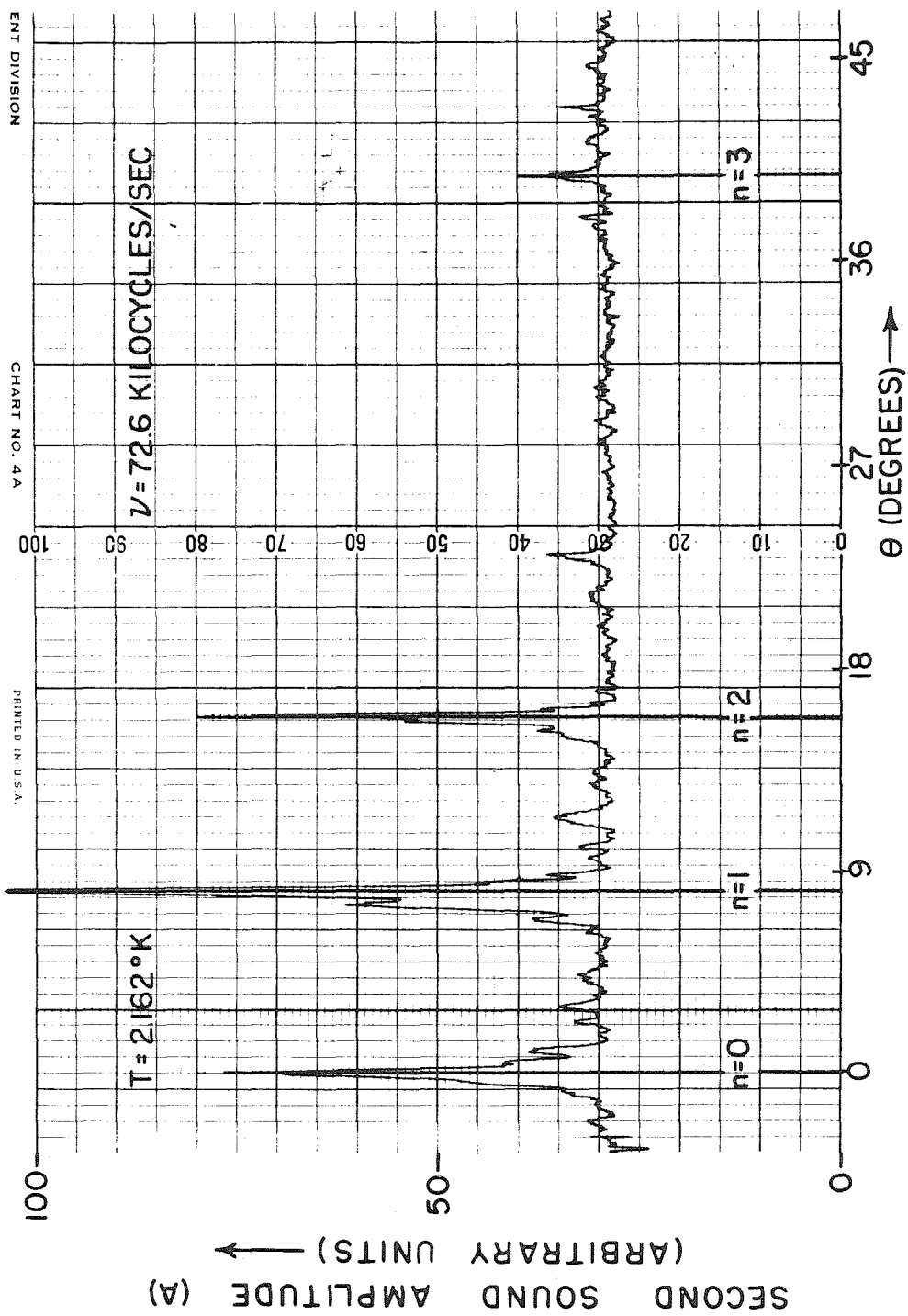
EXPERIMENTAL SECOND SOUND DIFFRACTION PATTERN
SECOND SOUND AMPLITUDE (A)
(ARBITRARY UNITS)
θ (DEGREES)
T = 2.162°K
ν = 72.6 KILOCYCLES/SEC
n=0
n=1
n=2
n=3
CHART NO. 4A
PRINTED IN U.S.A.

Figure 7(d)

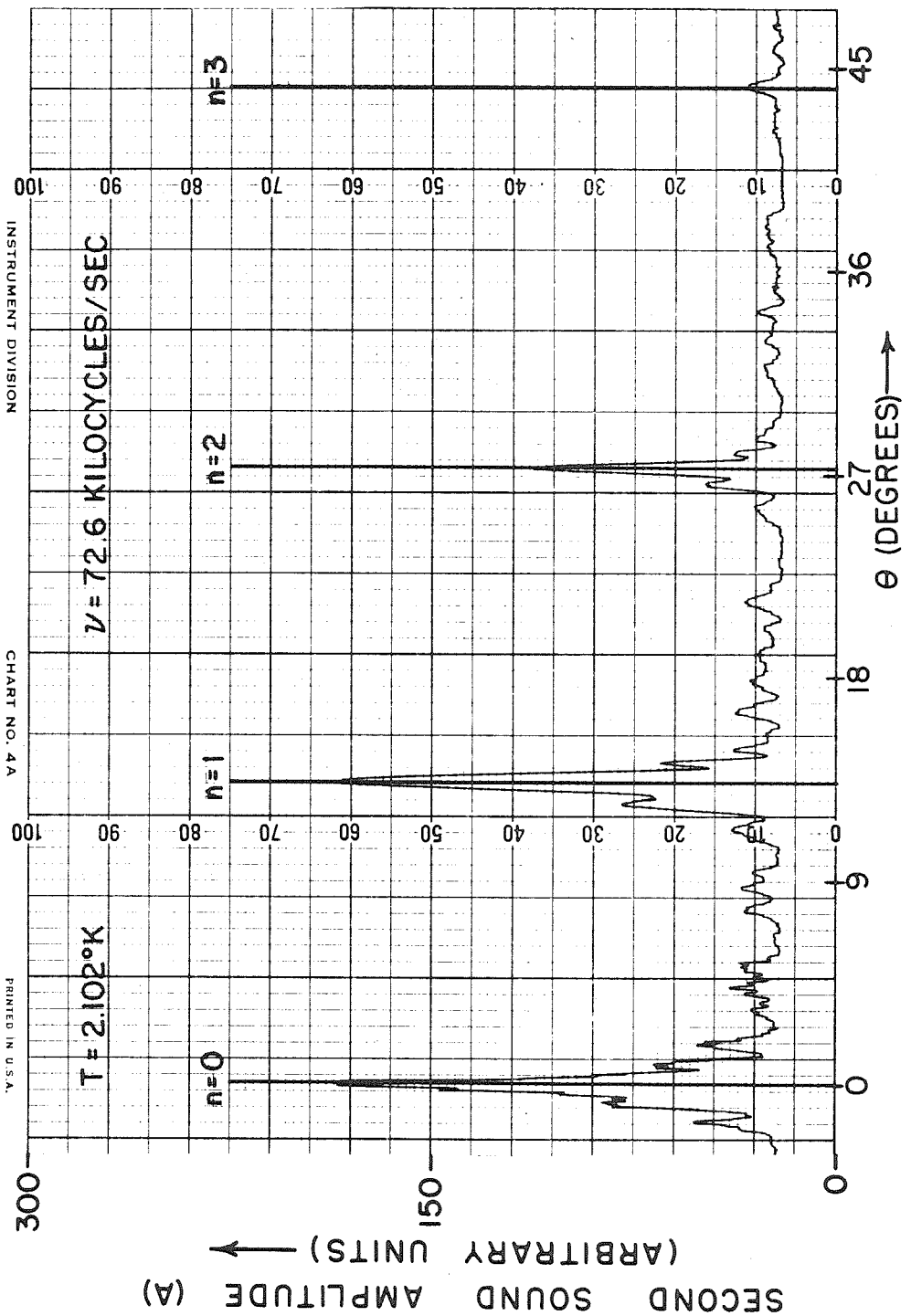

EXPERIMENTAL SECOND SOUND DIFFRACTION PATTERN

Figure 7(e)

EXPERIMENTAL SECOND SOUND DIFFRACTION PATTERN
SECOND SOUND AMPLITUDE (A)
(ARBITRARY UNITS)
1000
500
0
θ (DEGREES)
0
9
18
27
36
45
0
10
20
30
40
50
60
70
80
90
100
n=0
n=1
n=2
T = 1.395°K
ν = 72.6 KILOCYCLES/SEC
VARIAN ASSOCIATES, PALO ALTO, CALIF.
PRINTED IN U.S.A.

Figure 7(f)

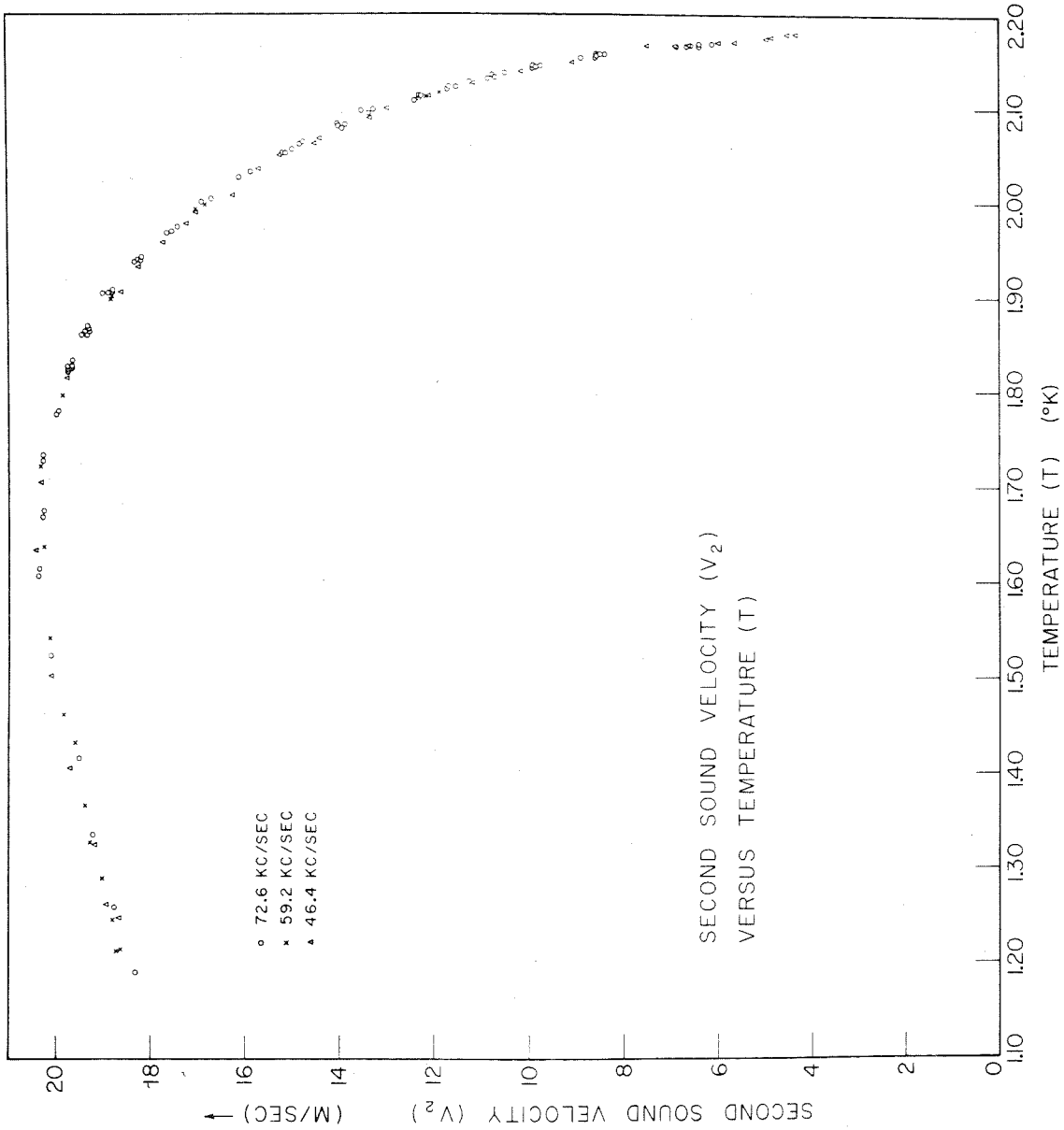
SECOND SOUND VELOCITY (V2) (M/SEC)
SECOND SOUND VELOCITY (V2)
VERSUS TEMPERATURE (T)
TEMPERATURE (T) (°K)
o 72.6 KC/SEC
× 59.2 KC/SEC
▲ 46.4 KC/SEC
0
2
4
6
8
10
12
14
16
18
20
1.10
1.20
1.30
1.40
1.50
1.60
1.70
1.80
1.90
2.00
2.10
2.20

Fig. 8

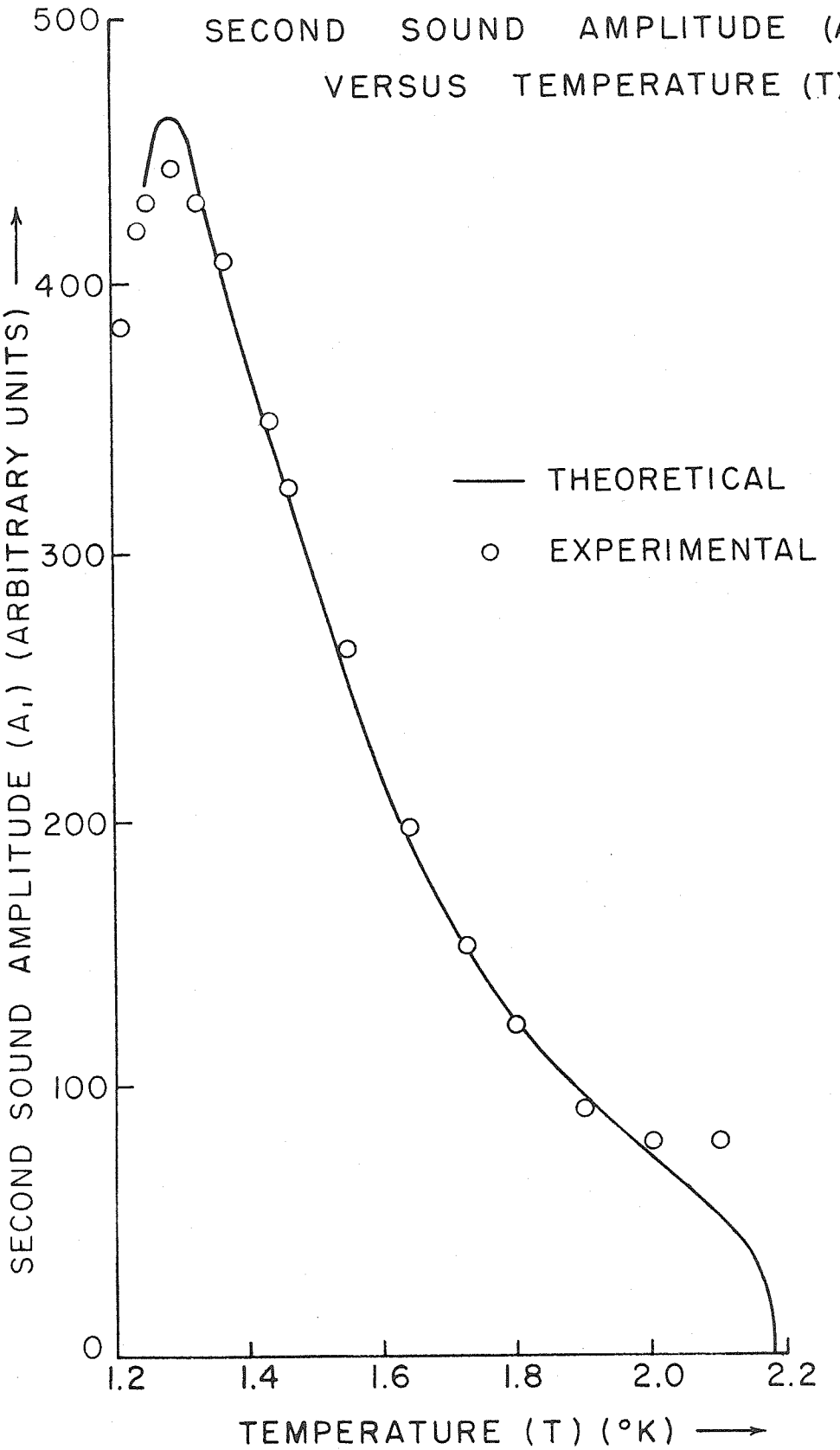
SECOND SOUND AMPLITUDE (A_1)
VERSUS TEMPERATURE (T)
SECOND SOUND AMPLITUDE (A_1) (ARBITRARY UNITS)
500
400
300
200
100
0
THEORETICAL
EXPERIMENTAL
1.2
1.4
1.6
1.8
2.0
2.2
TEMPERATURE (T) (°K)

Figure 9

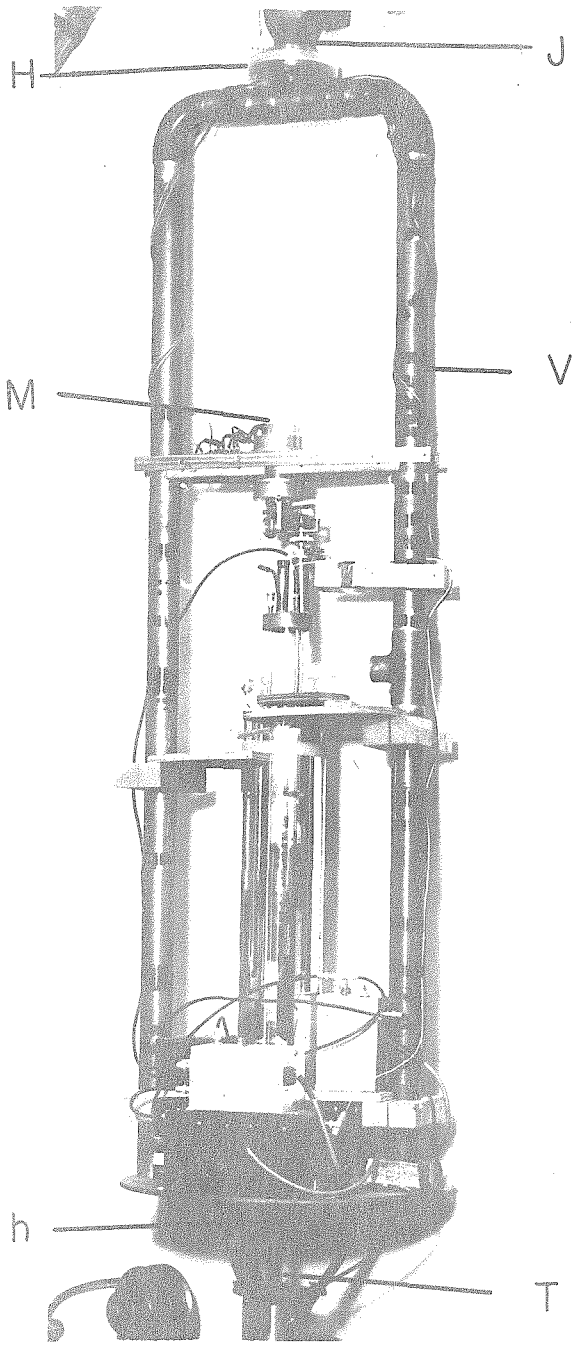

ROTATING EQUIPMENT

Figure 10

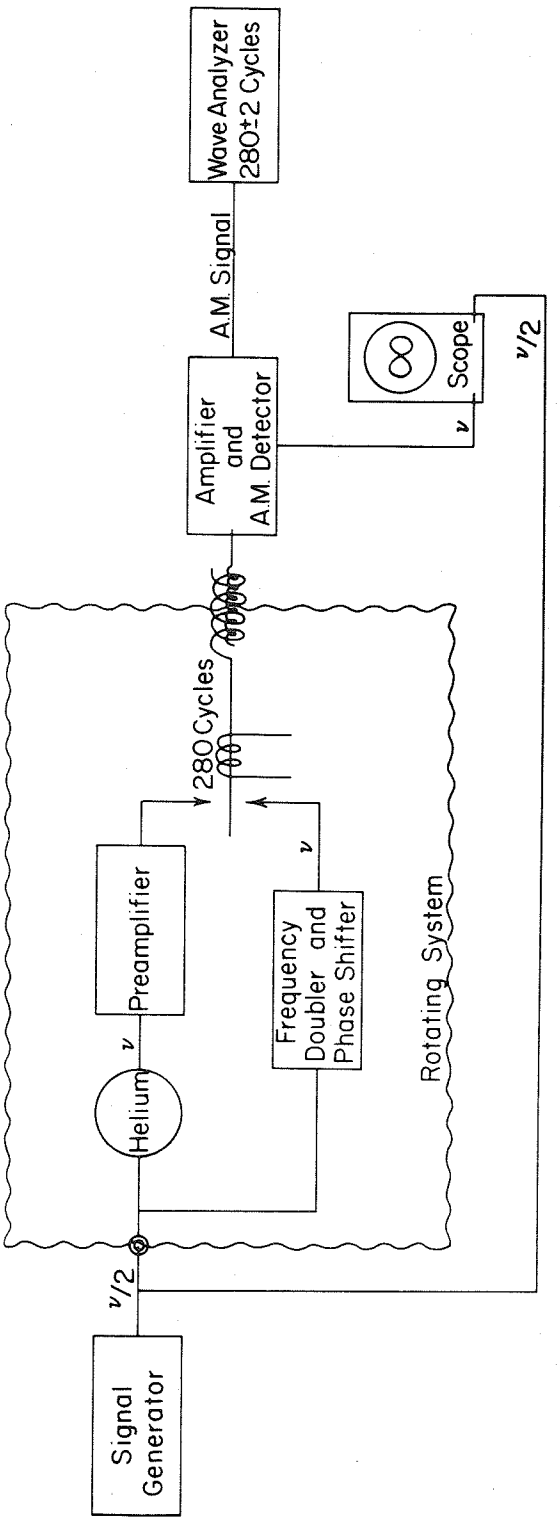

SCHEMATIC OF ELECTRONIC SYSTEM

Figure 11

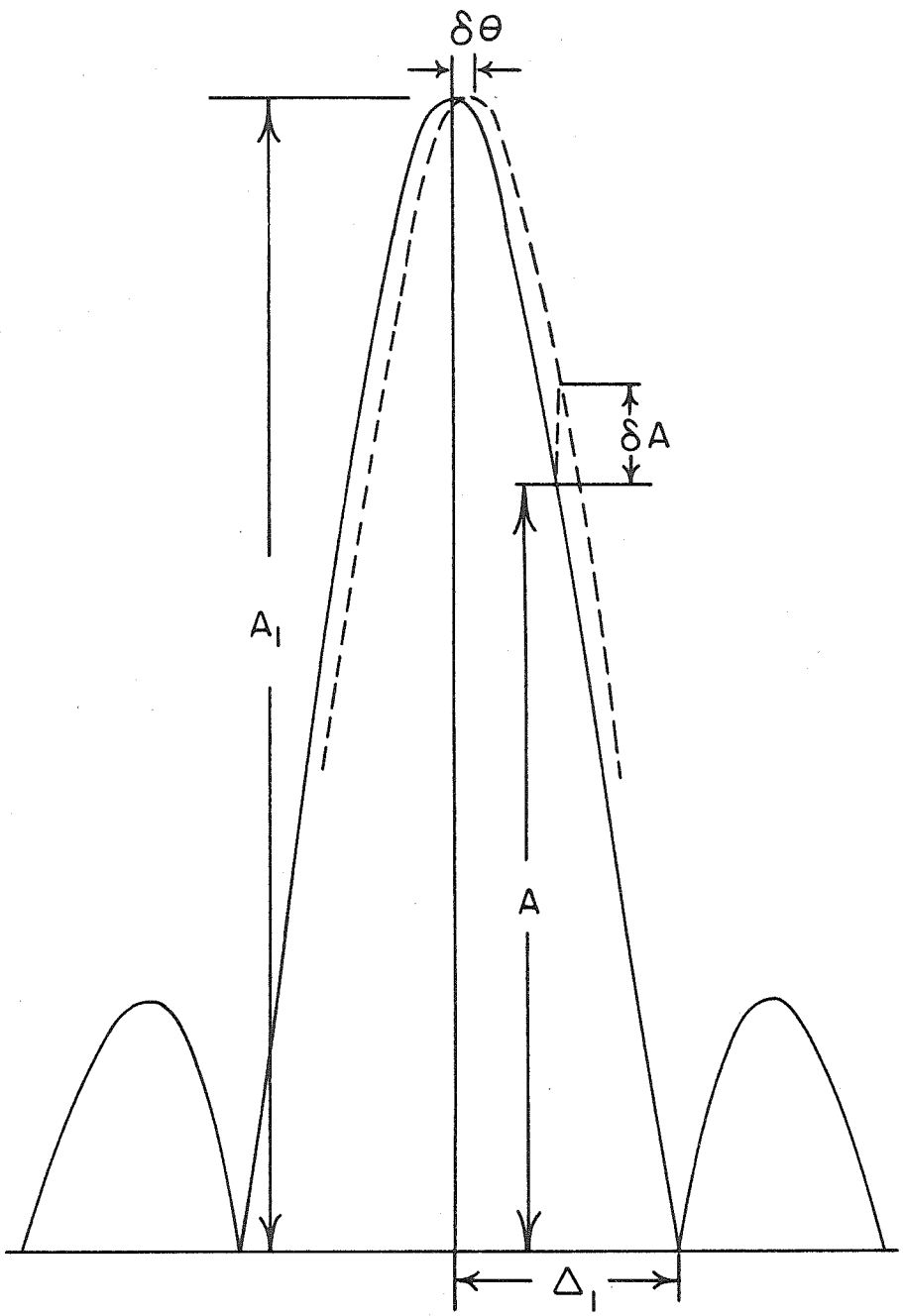

DEFINITION OF EXPERIMENTAL PARAMETERS

Figure 12

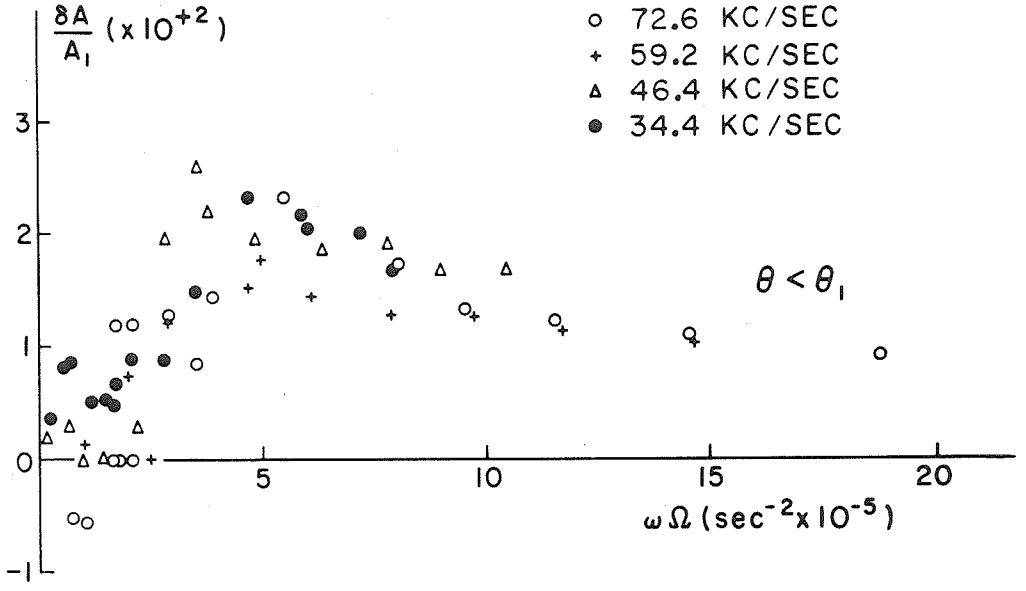

EXPERIMENTAL CHANGE IN SECOND SOUND SIGNAL LEVEL UPON ROTATION

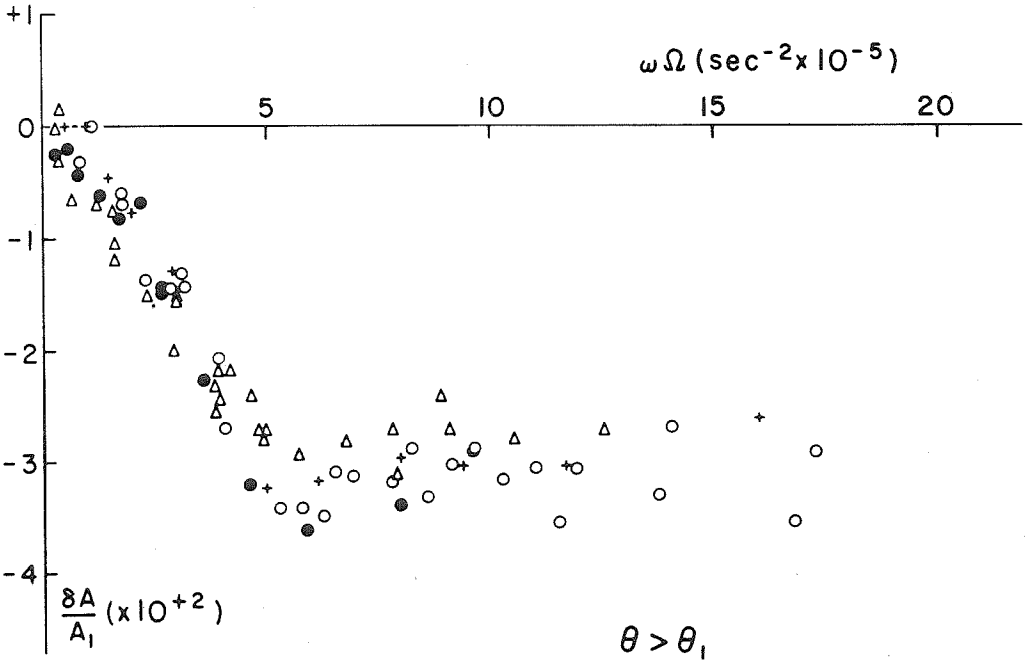

Fig. 13

EXAMPLE OF EXPERIMENTAL MEASUREMENT

Figure 14

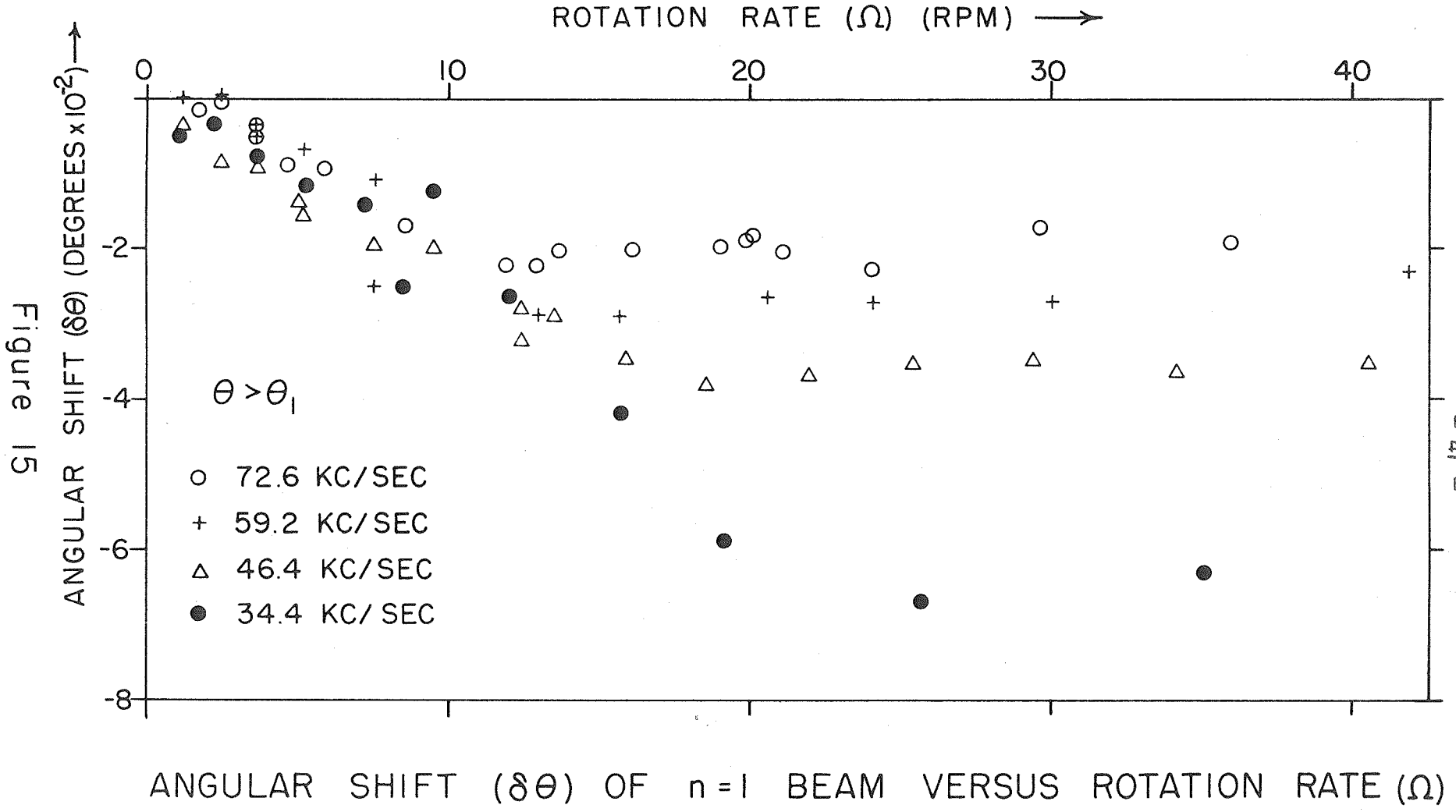

Figure 15

ANGULAR SHIFT (δθ) OF n = 1 BEAM VERSUS ROTATION RATE (Ω)

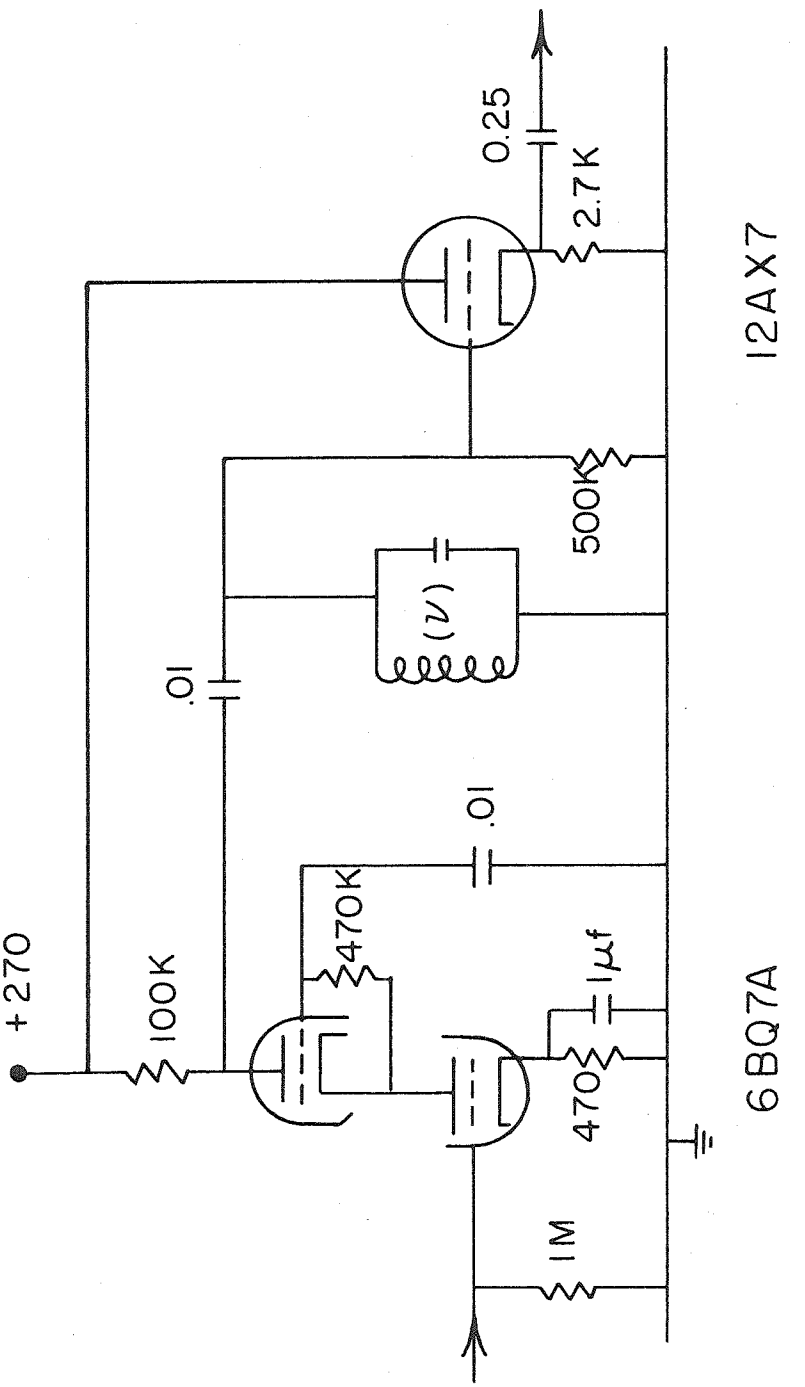
PREAMPLIFIER CIRCUIT
12AX7
6BQ7A
+270
100K
.01
470K
.01
1μf
470
1M
500K
0.25
2.7K
(V)

Fig. 16

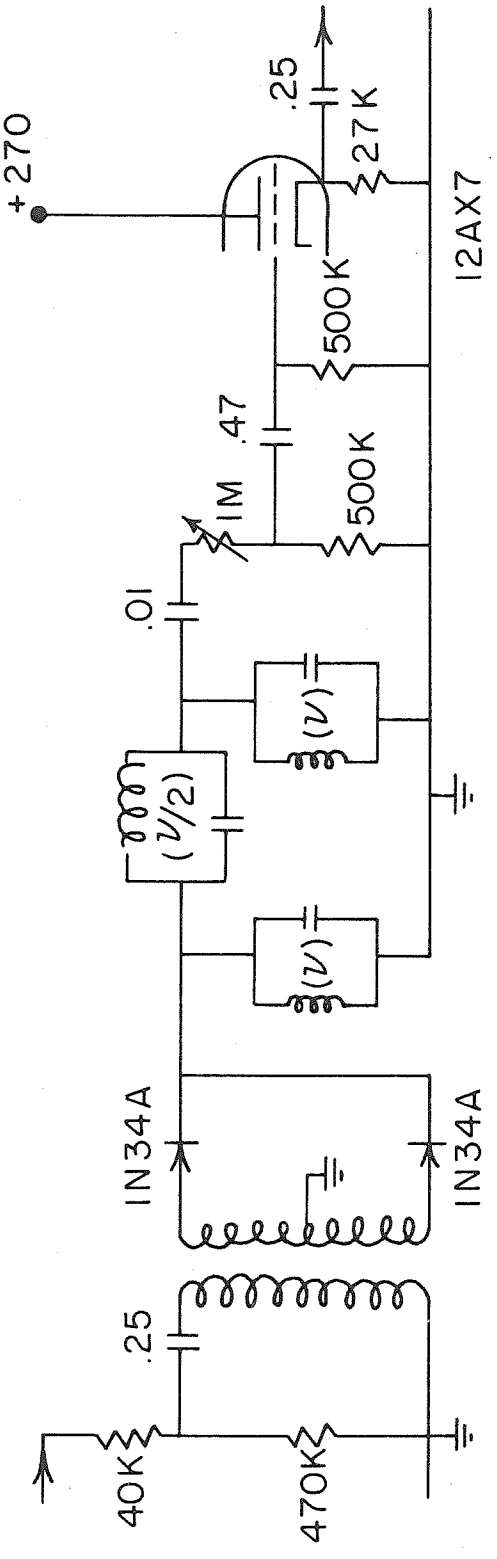

FREQUENCY DOUBLING CIRCUIT

Fig. 17

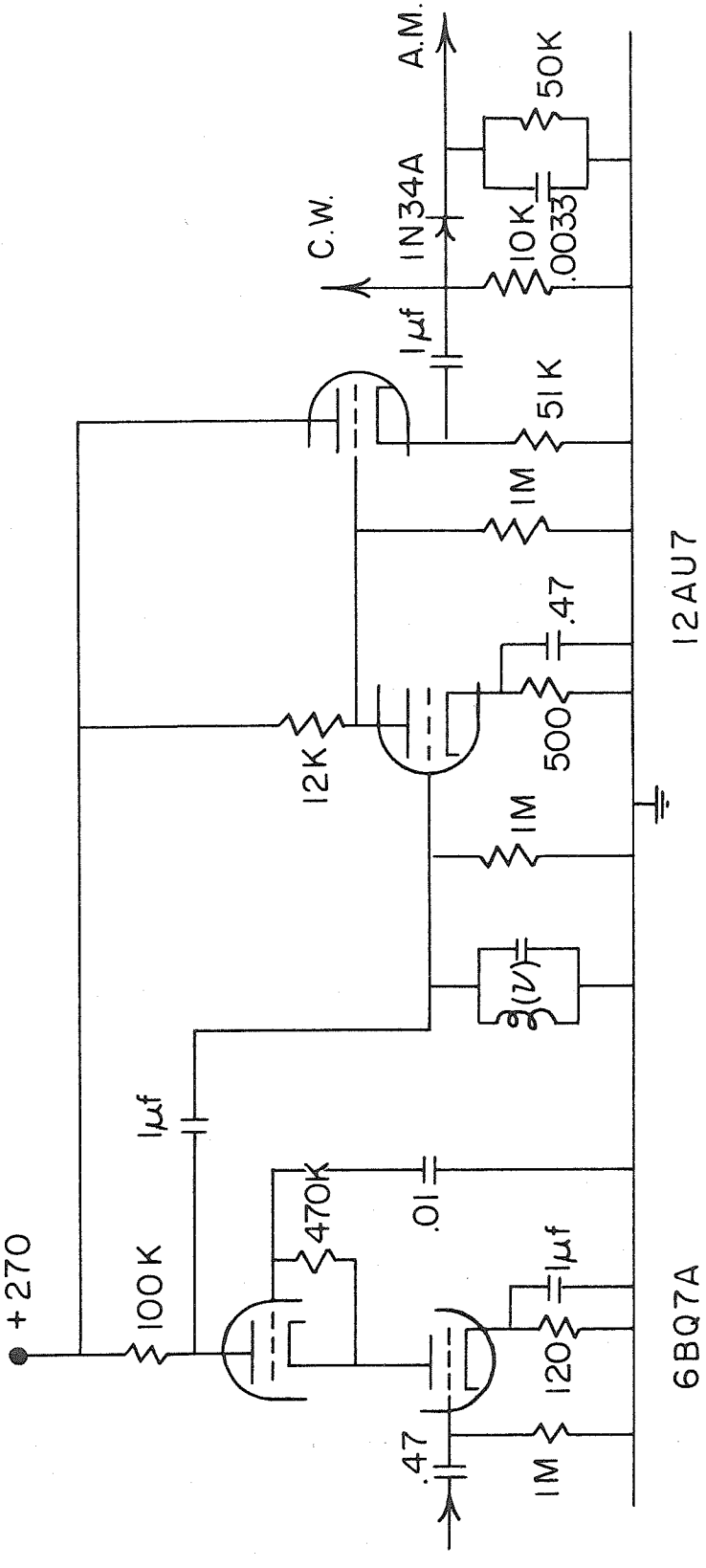

Fig. 18

AMPLIFIER AND A.M. DETECTOR CIRCUIT

REFERENCES

1) London, F., Nature, 141, 643 (1938); Phys. Rev. 54, 947 (1938)

2) Einstein, A., Ber. Berl. Akad., 261 (1924); 3 (1925)

3) Tisza, L., Phys. Rev. 72, 838 (1947)

4) Landau, L., J. Phys. (USSR) 5, 71 (1941)

5) Feynman, R.P., Progress in Low Temp. Phys., Vol. I, chapter II, C.J. Gorter editor, North Holland Publishing Co., Amsterdam (1955)

6) Peshkov, V., J. Physics (USSR) 8, 381 (1944)

7) Pellam, J.R., Phys. Rev. 74, 841 (1948)

8) Hanson, W.B. and Pellam, J.R., Phys. Rev. 95, 321 (1954)

9) Jenkins and White, Fundamentals of Optics, chapter 17, McGraw-Hill Book Company, New York (1950)

10) Peshkov, V., J. Phys. (USSR), 10, 389 (1946)
Pellam, J.R., Phys. Rev., 75, 1183 (1949)

11) Kramers, H., Wascher, J., Gorter, C., Physica, 18, 329 (1952)

12) Osborn, D.V., Proc. Roy. Soc. A, 63, 909 (1950)
Andronikashvili, E.L. and Kaverkin, I.P., J.E.T.P., 28, 126 (1955)

13) Hall, H.E., Conference of Low Temperature Physics, Paris 1955, p.63

14) Walmsley, R.H. and Lane, C.T., Phys. Rev., 112, 1041 (1958)

15) Vinen, W.F., Nature, 181, 1524 (1958)
Hall, H.E., Proc. Roy. Soc. (London), 245, 546 (1958)

16) Onsager, L., Nuov. Cim., Suppl. 2, 6, 249 (1949)